cients of the second-degree terms are small compared with those of the linear terms. Although a similar argument would establish that the second and third terms in eqn. 3*b* give rise to a second-order polynomial, the first term generates an infinite series in Φ_s. To minimise the number of surface patches required for a given degree of convergence, it is important to choose an integration grid co-ordinate system that gives the best linear approximation to g.

Results: Two examples will be considered: an offset paraboloidal reflector and an offset ellipsoidal reflector. With reference to Fig. 1, the parameters for the paraboloidal reflector

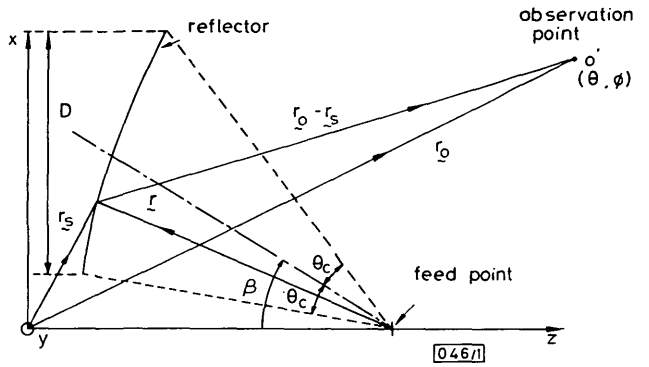

Fig. 1 *Reflector geometry*

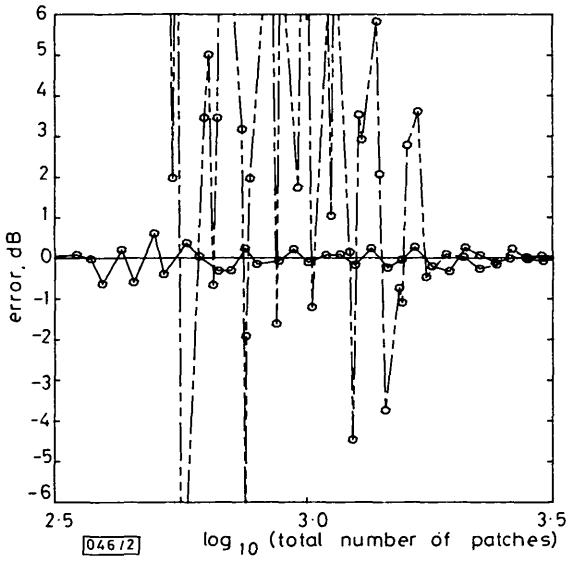

Fig. 2 *Convergence plot for offset paraboloidal reflector*
——— cartesian grid
----- polar grid

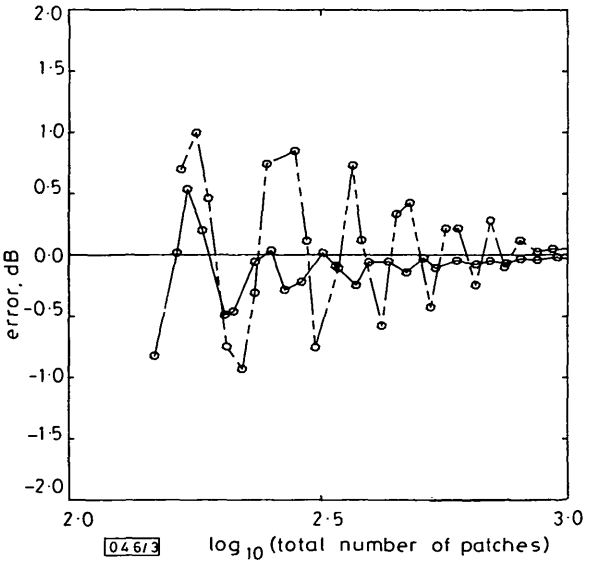

Fig. 3 *Convergence plot for offset ellipsoidal reflector*
——— cartesian grid
----- polar grid

are $\beta = 44°$, $\varphi_c = 30°$, $D = 150\lambda$ and $F = 114\lambda$ (focal length). The ellipsoidal reflector has parameters $\beta = -16°$, $\varphi_c = 14°$, $a = 47\lambda$ (major axis), $b = 38{\cdot}5\lambda$ (minor axis) and $D = 28\lambda$. The primary feed is linearly polarised and is modelled to radiate a rotationally symmetric field. The feed taper is -12 dB at the edge of the paraboloidal reflector and -17 dB at the edge of the ellipsoidal reflector. The error in $|E(\theta, \Phi)|$, with respect to the converged value, is shown in Figs. 2 and 3 for the paraboloidal and ellipsoidal reflectors, respectively. The observation point in Fig. 2 is taken at a sidelobe maximum $\theta = 19{\cdot}4°$, $\Phi = 90°$, and in Fig. 3 at $\theta = 60°$, $\Phi = 0°$, which lies in the main scattered beam. The ratio of radial to azimuthal patches in the polar grid was taken as $\Delta\rho_s/\Delta\Phi_s = 0{\cdot}318D$, which was found to be an optimum, whereas for the cartesian grid $\Delta x_s/\Delta y_s = 1$. Since the time taken to evaluate the integral over a patch is approximately the same for both co-ordinate systems, the total number of patches is directly proportional to the computation time.

For the case of both the paraboloidal and ellipsoidal reflectors the convergence obtained with the cartesian grid is clearly superior to that of the polar grid. With the ellipsoidal reflector the linear approximation to the term $Z_s(x_s, y_s)\cos\theta - r$ in cartesian co-ordinates is less good than for the paraboloidal reflector. However, the approximation to g is better than for polar co-ordinates, and hence the convergence is improved.

Acknowledgment: The authors are indebted to Dr. T. S. M. Maclean for discussions relating to this letter.

J. R. PARKINSON
M. J. MEHLER
Department of Electronic & Electrical Engineering
University of Birmingham
PO Box 363
Birmingham B15 2TT, United Kingdom

10th July 1986

References

1 SILVER, S.: 'Microwave antenna theory and design'. IEE electromagnetic waves series 19 (Peter Peregrinus Ltd., London, 1984)
2 LUDWIG, A. C.: 'Computation of radiation patterns involving numerical double data integration', *IEEE Trans.*, 1968, **AP-16**, pp. 767–769

BIQUADRATIC FILTER SECTIONS EMPLOYING A SINGLE CURRENT CONVEYOR

Indexing terms: Filters, Active filters, Current conveyors, Circuit theory and design

LP, BP and HP filters with low passive component sensitivity and independently adjustable ω_0 or Q are presented. In addition, two new types of current conveyor are introduced and a new current-conveyor classification is proposed.

Introduction: The concept of current conveying was introduced by Smith and Sedra in 1968.[1] One important application of the current conveyor (CC) has been in the implementation of filters, where it has been shown by Aronhime,[2] Senani[3] and many others that the CC can be used to implement nearly all voltage-transfer functions.

The main aim of this letter is to introduce two additional types of CC which are useful for implementing biquadratic filters, and a correspondingly new way of classifying CCs.

Biquads using current conveyor: Consider the four-variable configuration shown in Fig. 1 (without Z_5).

The CC in Fig. 1 can be either CCII+ or CCII−, and all the impedances Z_1, Z_2, Z_3 and Z_4 can be resistive, inductive, capacitive,* FDNR* or other.

* With some restriction due to the need for a DC bias path

Simple analysis shows that the four-variable configuration has the following voltage transfer function:

$$\frac{V_o}{V_i} = \frac{Z_1 Z_4}{k(Z_1 Z_4 + Z_2 Z_4 + Z_3 Z_4 \pm Z_1 Z_2)} \quad (1)$$

The negative sign in eqn. 1 corresponds to the use of CCII+ while the positive is for CCII−.

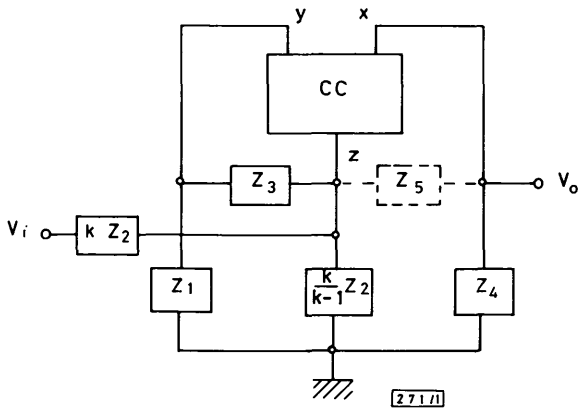

Fig. 1 *Four- or five-variable configuration*

Since a filter should have all of its natural modes in the left halfplane, the negative four-variable configuration is more suitable for filter implementations.

As an example, we choose $Z_1 = 1/C_1 s$, $Z_2 = 1/C_2 s$, $Z_3 = R_3$ and $Z_4 = R_4$ for the negative four-variable configuration. This results in the following bandpass voltage transfer function:

$$\frac{V_o}{V_i} = \frac{R_4 C_2 s}{k[R_3 R_4 C_1 C_2 s^2 + R_1(C_1 + C_2)s + 1]} \quad (2)$$

Thus

$$\omega_0 = 1/\sqrt{(R_3 R_4 C_1 C_2)} \quad (3)$$

and

$$\omega_0/Q = (C_1 + C_2)/R_3 C_1 C_2 \quad (4)$$

Note that ω_0 can be adjusted independently of ω_0/Q by changing the value of R_4. Sensitivity analysis of the filter shows that

$$S^{\omega_0}_{R_3} = S^{\omega_0}_{R_4} = S^{\omega_0}_{C_1} = S^{\omega_0}_{C_2} = -S^{Q}_{R_3} = -S^{Q}_{R_4} = -1/2$$

$$S^{Q}_{C_1} = -S^{Q}_{C_2} = \frac{1}{2}\left(\frac{C_2 - C_1}{C_2 + C_1}\right)$$

Therefore, the sensitivities of ω_0 and Q to passive components are small if $C_1 \simeq C_2$.

It was found to be impossible to design LP and HP filters using the four-variable configuration and only resistive and capacitive impedances. As a result, the five-variable configuration shown in Fig. 1 (with Z_5) is introduced.

Simple analysis shows that

$$\frac{V_o}{V_i} = \frac{Z_1 Z_4 Z_5}{k(Z_1 Z_4 Z_5 + 2Z_2 Z_3 Z_4 + Z_2 Z_4 Z_5 + Z_3 Z_4 Z_5 - Z_1 Z_2 Z_5)} \quad (5)$$

when CCII+ is used and

$$\frac{V_o}{V_i} = \frac{Z_1 Z_4}{k(Z_1 Z_4 + Z_2 Z_4 + Z_3 Z_4 + Z_1 Z_2)} \quad (6)$$

when CCII− is used.

Note that the fact the variable Z_5 does not appear in eqn. 6 defeats the purpose of adding Z_5, which is to provide another degree of freedom in the choice of impedences in the circuit configuration. However, if we define a new type of negative CC which inverts the polarity of voltage at terminal x instead of the direction of current at terminal z (see Fig. 2), and use it in the five-variable configuration, some useful results are

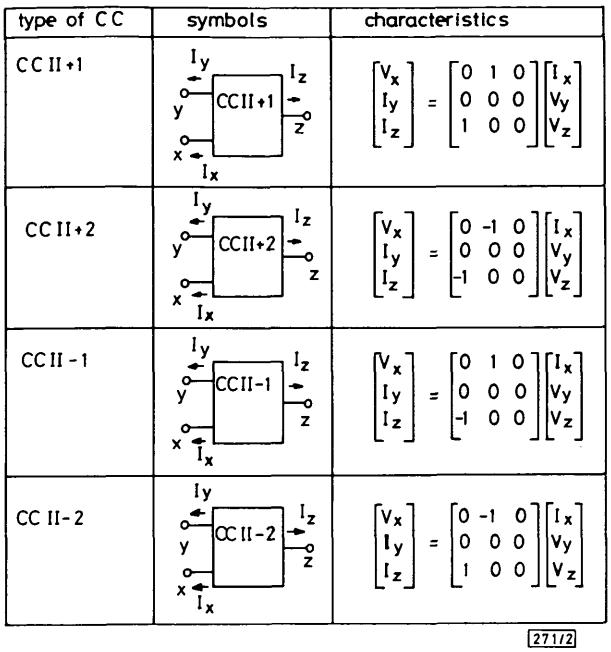

Fig. 2 *New current conveyor classification*

obtained. This new negative CC is called here a second-generation negative type-2 current conveyor, or CCII−2.

Using CCII−2 in the five-variable configuration produces the following voltage transfer function:

$$\frac{V_o}{V_i} = \frac{Z_1 Z_4 Z_5}{k(4Z_1 Z_2 Z_4 + Z_1 Z_2 Z_5 + Z_1 Z_4 Z_5 + 2Z_2 Z_3 Z_4 + Z_2 Z_4 Z_5 + Z_3 Z_4 Z_5)} \quad (7)$$

If we choose $Z_1 = 1/C_1 s$, $Z_2 = R_2$, $Z_3 = R_3$, $Z_4 = R_4$ and $Z_5 = 1/C_5 s$, then

$$\frac{V_o}{V_i} = \frac{R_4}{k(Ds^2 + Es + F)} \quad (8)$$

where

$$D = 2R_2 R_3 R_4 C_1 C_5$$

$$E = 4R_2 R_4 C_5 + R_2 R_4 C_1 + R_3 R_4 C_1$$

$$F = R_2 + R_4$$

which corresponds to the transfer function of an LP filter with

$$\omega_0 = \sqrt{[(R_2 + R_4)/2R_2 R_3 R_4 C_1 C_5]} \quad (9)$$

and

$$\omega_0/Q = E/D \quad (10)$$

Again, note that ω_0 can be adjusted independently of ω_0/Q by changing the value of R_4. Sensitivity analysis shows that

$$S^{\omega_0}_{R_3} = S^{\omega_0}_{R_1} = S^{\omega_0}_{C_5} = -1/2 \qquad \tfrac{1}{2} < S^{Q}_{R_4} < \tfrac{3}{4}$$

and

$$-S^{\omega_0}_{R_2},\ -S^{\omega_0}_{R_4},\ S^{Q}_{R_2},\ S^{Q}_{R_3},\ S^{Q}_{C_1},\ S^{Q}_{C_5} < 1/2$$

As a last example, if we choose $Z_1 = R_1$, $Z_2 = 1/C_2 s$, $Z_3 = 1/C_3 s$, $Z_4 = R_4$ and $Z_5 = R_5$, then

$$\frac{V_o}{V_i} = \frac{R_1 R_4 R_5 C_2 C_3 s^2}{k(Gs^2 + Hs + I)} \quad (11)$$

where

$$G = R_1 R_4 R_5 C_2 C_3$$

$$H = (4R_1 R_4 + R_1 R_5 + R_4 R_5) C_3 + R_4 R_5 C_2$$

$$I = 2R_4$$

which corresponds to the transfer function of an HP filter with

$$\omega_0 = \sqrt{(2/R_1 R_2 C_2 C_3)} \tag{12}$$

and

$$\omega_0/Q = H/G \tag{13}$$

Note that we can adjust ω_0/Q by changing the value of R_4, without affecting ω_0. Sensitivity analysis yields the following results:

$$S^{\omega_0}_{R_1} = S^{\omega_0}_{R_5} = S^{\omega_0}_{C_2} = S^{\omega_0}_{C_3} = -1/2$$

$$S^{Q}_{R_1}, S^{Q}_{R_5}, S^{Q}_{C_2}, S^{Q}_{C_3} < 1/2 \qquad S^{Q}_{R_4} \ll 1$$

Finally, a new CC classification is proposed as shown in Fig. 2.

Conclusion: In this letter BP, HP and LP filters employing a single CCII are presented. In all cases the value of k (attenuation factor), ω_0 and Q are independently adjustable. Moreover, all three filters exhibit low passive-component sensitivity. Two additional types of CC and a correspondingly new way of classifying CCs in general are also introduced.

C. P. CHONG
K. C. SMITH

Department of Electrical Engineering
University of Toronto
Toronto, Ontario, Canada M5S 1A1

29th August 1986

References

1 SMITH, K. C., and SEDRA, A.: 'The current conveyor: a new circuit building block', *Proc. IEEE*, 1968, **56**, pp. 1368–1369
2 ARONHIME, P.: 'Transfer function synthesis using a current conveyor', *IEEE Trans.*, 1974, **CAS-21**, pp. 312–313
3 SENAI, R.: 'Novel higher-order active filter design using current conveyors', *Electron. Lett.*, 1985, **21**, pp. 1055–1057

PAIR-GROOVE-SUBSTRATE GaAs/AlGaAs MULTIQUANTUM-WELL LASERS WITH A SELF-ALIGNED STRIPE GEOMETRY

Indexing term: Semiconductor lasers

GaAs/AlGaAs multiquantum-well (MQW) lasers with a self-aligned structure incorporating a waveguide and current confinement were fabricated on a substrate with a pair of etched grooves using two-step epitaxial growth. First, a current-blocking layer was grown selectively on the substrate by low-pressure organometallic vapour-phase epitaxy (OMVPE), and then the GaAs/AlGaAs MQW laser structure was constructed on the substrate with the OMVPE layer by molecular-beam epitaxy. The mesa-shaped part of the active layer above the current-confinement region provides a lateral refractive-index optical waveguide. The lasers show well controlled transverse-mode oscillations with low threshold currents.

Single- and multiquantum-well (MQW) lasers have been developed by molecular-beam epitaxy (MBE) and organometallic vapour-phase epitaxy (OMVPE), and have shown low threshold current densities[1,2] and weak temperature dependence of the threshold current.[3] However, few self-aligned structures[4–6] of quantum-well lasers have been proposed in which waveguiding and current confinement are accomplished in a self-aligned manner.

We have developed pair-groove-substrate (PGS) GaAs/AlGaAs MQW lasers, which have a refractive-index guided structure formed on the substrate with a pair of grooves, and show excellent characteristics, such as low threshold currents and stable fundamental transverse-mode oscillations.[7] However, it is difficult in these lasers to align the current confinement region to the optical confinement region, because the current confinement region is formed by selectively diffusing zinc after the growth.

In this letter we report self-aligned PGS GaAs/AlGaAs MQW lasers with an inner current-blocking layer. The current-blocking layer is formed using selective growth by low-pressure OMVPE.[8]

A scanning electron micrograph of the cross-section and a schematic drawing of the slef-aligned PGS MQW laser are shown in Fig. 1. The fabrication process of this laser was as

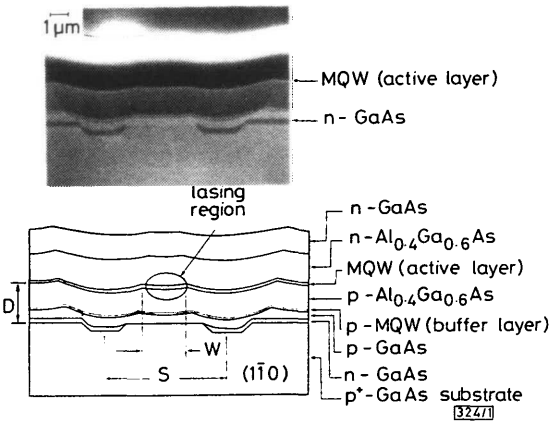

Fig. 1 *Scanning electron micrograph of laser cross-section (top) and schematic drawing (bottom) of laser structure*

follows. An Si_3N_4 insulator film was formed on a Zn-doped (001) p^+-GaAs substrate by chemical vapour deposition. A pair of stripes were opened in the insulator film along the $\langle 1\bar{1}0 \rangle$ direction by conventional photolithography, and then a pair of grooves were formed by chemically etching the opened stripe regions of the substrate. As a result, a mesa was formed between the grooves. The grooves had slanting planes of {111}A perpendicular to the (1$\bar{1}$0) plane. The insulator film mask outside the mesa was preferentially etched off and then 0·4 μm-thick n-GaAs (Si-doped, $n \sim 1 \times 10^{18}\,cm^{-3}$) was selectively grown[8] as a current blocking layer on the substrate by low-pressure OMVPE. The growth was performed under a V/III mole ratio of 75 and a substrate temperature of 650°C. The epitaxial GaAs layer grew only on the unmasked area, and no ridge growth occurred near the insulator film edge on the substrate.[8] After removing the insulator film mask, the GaAs/AlGaAs MQW laser structure was constructed by MBE on the substrate as shown in Fig. 1. The MQW active layer, which is sandwiched between a p-$Al_{0.4}Ga_{0.6}As$ cladding layer (Be-doped, $p \sim 1 \times 10^{18}\,cm^{-3}$, 1·4 μm thick) and an n-$Al_{0.4}Ga_{0.6}As$ (Si-doped, $n \sim 1 \times 10^{18}\,cm^{-3}$, 1·4 μm thick) cladding layer, consists of six 100 Å-thick GaAs wells separated by five 50 Å-thick $Al_{0.2}Ga_{0.8}As$ barriers. A p-MQW buffer layer, which improves the quality of the succeeding grown layers, consists of 10 periods of 100 Å-thick GaAs ($p \sim 2 \times 10^{18}\,cm^{-3}$) alternating with 100 Å-thick $Al_{0.4}Ga_{0.6}As$ ($p \sim 1 \times 10^{18}\,cm^{-3}$). These GaAs/AlGaAs epitaxial layers were grown by MBE at a substrate temperature of 750°C, with a substrate rotation rate of 5 rev/min and a growth rate of 0·9 μm/h for GaAs. After the MBE growth, the substrate was lapped. Then, Au-Ge/Au and Au-Zn/Au were evaporated for n- and p-side contacts, respectively.

In this laser, the mesa-shaped part consisting of the active and cladding layers provides a lateral refractive-index waveguide. Since the mesa-shaped part is formed above the current confinement region separating the current-blocking layers, the lateral waveguide is self-aligned to the current confinement